

An intersectional viral-genetic method for fluorescent tracing of axon collaterals reveals details of noradrenergic locus coeruleus structure

<https://doi.org/10.1523/ENEURO.0010-20.2020>

Cite as: eNeuro 2020; 10.1523/ENEURO.0010-20.2020

Received: 9 January 2020

Revised: 9 April 2020

Accepted: 27 April 2020

This Early Release article has been peer-reviewed and accepted, but has not been through the composition and copyediting processes. The final version may differ slightly in style or formatting and will contain links to any extended data.

Alerts: Sign up at www.eneuro.org/alerts to receive customized email alerts when the fully formatted version of this article is published.

Copyright © 2020 Plummer et al.

This is an open-access article distributed under the terms of the Creative Commons Attribution 4.0 International license, which permits unrestricted use, distribution and reproduction in any medium provided that the original work is properly attributed.

An intersectional viral-genetic method for fluorescent tracing of axon collaterals reveals details of noradrenergic locus coeruleus structure

Abbreviated title:

Tracing LC-NE axon collaterals

Authors:

Nicholas W. Plummer^{1*}, Daniel J. Chandler^{2*}, Jeanne M. Powell¹, Erica L. Scappini³, Barry D. Waterhouse^{2†}, Patricia Jensen^{1†}

Author affiliations:

¹Neurobiology Laboratory, National Institute of Environmental Health Sciences, National Institutes of Health, Department of Health and Human Services, Research Triangle Park, NC 27709, USA.

²Department of Cell Biology and Neuroscience, Rowan University School of Osteopathic Medicine, Stratford, NJ 08084, USA.

³Signal Transduction Laboratory, National Institute of Environmental Health Sciences, National Institutes of Health, Department of Health and Human Services, Research Triangle Park, NC 27709, USA.

*These authors contributed equally

†Corresponding authors

Author Contributions:

PJ conceived method. NWP, DJC, BDW and PJ designed experiments. NWP, DJC, JMP, and ELS performed research. NWP, DJC, JMP, ELS, BDW and PJ analyzed data. NWP and PJ created figures. NWP, DJC, BDW and PJ wrote the paper.

Correspondence should be addressed to:

Patricia Jensen; patricia.jensen@nih.gov

Barry D. Waterhouse; waterhouse@rowan.edu

Number of figures: 6

Number of tables: 1

Number of multimedia: 0

Number of Words for abstract: 182

Number of Words for Significance Statement: 110

Number of Words for Introduction: 663

Number of Words for Discussion: 1093

Acknowledgements:

The authors thank Eric J. Kremer (Institut de Génétique Moléculaire de Montpellier) for providing the Cav2-Cre virus. We thank the NIEHS Comparative Medicine Branch and the NIEHS Fluorescence Microscopy and Imaging Center for valuable support.

Conflict of interest statement:

Authors report no conflict of interest.

Funding sources:

This research was funded by the Intramural Research Program of the US National Institutes of Health, National Institute of Environmental Health Sciences (ZIA-ES-102805 to PJ) and by the Extramural Research Program of the US National Institutes of Health, National Institute of Mental Health (1R01MH101178-01A1 to BDW).

ABSTRACT

Understanding the function of broadly projecting neurons depends on comprehensive knowledge of the distribution and targets of their axon collaterals. While retrograde tracers and, more recently, retrograde viral vectors have been used to identify efferent projections, they have limited ability to reveal the full pattern of axon collaterals from complex, heterogeneous neuronal populations. Here we describe TrAC (Tracing Axon Collaterals), an intersectional recombinase-based viral-genetic strategy that allows simultaneous visualization of axons from a genetically defined neuronal population and a projection-based subpopulation. To test this new method, we have applied TrAC to analysis of locus coeruleus norepinephrine (LC-NE)-containing neurons projecting to medial prefrontal cortex (mPFC) and primary motor cortex (M1) in laboratory mice. TrAC allowed us to label each projection-based LC-NE subpopulation, together with all remaining LC-NE neurons, in isolation from other noradrenergic populations. This analysis revealed mPFC- and M1-projecting LC-NE subpopulations differ from each other and from the LC as a whole in their patterns of axon collateralization. Thus, TrAC complements and extends existing axon tracing methods by permitting analyses that have not previously been possible with complex genetically defined neuronal populations.

SIGNIFICANCE STATEMENT

We have developed a new method for mapping axon collaterals of genetically defined neuronal subtypes. TrAC uses an intersectional genetic strategy to define a cell population of interest, and a retrograde viral construct to label a subpopulation based on its axonal projections. This method has three major benefits: 1) only one viral injection is required for labeling, 2) axons from a projection-based subpopulation can be visualized together with a broader genetically defined population, and 3) the cell population of interest can be defined by transient developmental genetic information. Our proof-of-principle analysis of noradrenergic

77 locus coeruleus projections to the forebrain extends previous analyses and reveals new details
78 of this complex system.

79

80 INTRODUCTION

81 Fundamental to our understanding of neural circuit dynamics and function is
82 comprehensive knowledge of the regions of the central nervous system (CNS) innervated by
83 neurochemically-identified cell types. While conventional anatomical tract tracing methods have
84 long been used to identify the afferent inputs and efferent projections of neuronal populations,
85 these traditional approaches have proven impractical for revealing the full distribution of axon
86 collaterals from a broadly projecting pool of neurons. One such brain region is the noradrenergic
87 nucleus locus coeruleus (LC), a brainstem nucleus which provides norepinephrine (NE) to
88 virtually the entire central nervous system. Early investigations into LC anatomy using
89 conventional tracing methods suggested that its cells possess highly ramified axons with the
90 potential to innervate broad regions of the CNS without regard for terminal field function (Bloom
91 et al., 1971; Foote et al., 1980; Foote et al., 1983; Aston-Jones et al., 1986; Loughlin et al.,
92 1986). Because of this apparent lack of functional organization, the LC has long been
93 considered a homogeneous entity with neurons that release NE globally, thus promoting
94 uniform actions throughout the brain and spinal cord simultaneously.

95 More recent evidence suggests that individual LC neurons innervate terminal fields in a
96 more discrete and orderly fashion than originally thought (Simpson et al., 1997; Howorth et al.,
97 2009; Chandler et al., 2014; Uematsu et al., 2015; Bellesi et al., 2016; Li et al., 2016; Hirschberg
98 et al., 2017; McCall et al., 2017; Plummer et al., 2017; Uematsu et al., 2017; Chandler et al.,
99 2019). For example, it has been shown that LC cells projecting to medial prefrontal cortex
100 (mPFC) are anatomically, molecularly, and electrophysiologically distinct from those that project
101 to primary motor cortex (M1) (Chandler et al., 2013; Chandler et al., 2014). Additionally,
102 injection of retrograde tracers into functionally related terminal fields (e.g. structures along the

103 ascending somatosensory pathway) results in a higher percentage of double-labeled LC-NE
104 neurons than when tracers are injected into functionally unrelated terminal fields (Simpson et
105 al., 1997).

106 Based on these findings, there is renewed interest in identifying the collateral projections
107 of the LC-NE system. Several laboratories have attempted to define the organizational
108 principles of this nucleus using a variety of novel approaches that have yielded conflicting
109 results. While some have provided evidence for a modularly organized LC with subpopulations
110 of neurons possessing limited axonal arborization confined to a small number of terminal fields
111 (Chandler et al., 2013; Chandler et al., 2014; Kebschull et al., 2016; Hirschberg et al., 2017;
112 Uematsu et al., 2017), others have reported highly collateralized LC axons that innervate many
113 functionally unrelated efferent targets (Schwarz et al., 2015). In order to resolve these
114 discrepancies and gain a better understanding of the functional circuit-level organization of the
115 LC, it is necessary to develop and apply methods that can faithfully identify the CNS regions
116 that receive collateral projections from LC-NE neurons projecting to a defined target. In a
117 system this complex, with other brainstem noradrenergic neuron populations projecting to many
118 of the same target sites, a method is required that can account for all LC-NE neurons without
119 labeling any other NE neuron populations.

120 Toward this goal, we developed a methodology termed TrAC (Tracing Axon Collaterals)
121 that combines intersectional recombinase-based genetics with retrograde viral delivery of a
122 recombinase to label axon collaterals from genetically-defined cell-types. Here we describe
123 TrAC and its application to reveal collateral networks of LC-NE neurons projecting to medial
124 prefrontal cortex (mPFC) or primary motor cortex (M1), demonstrating the utility of this approach
125 for dissecting the anatomy of complex, neurochemically identified neuronal populations. We
126 found that retrograde viral delivery of a recombinase into either terminal field region produced
127 similar numbers and distributions of retrogradely labeled LC neurons, but the patterns of axon
128 collateralization were not identical. The labeled neurons had dense projections to the site of

129 injection, with widespread, albeit sparse, collateral axons present in other cortical and
 130 subcortical targets. These findings are in general agreement with many other studies,
 131 suggesting that the LC-NE efferent pathway is functionally ordered and modular in design.

132

133 MATERIALS AND METHODS

134 Animals

135 This study was performed in accordance with the recommendations in the Guide for the
 136 Care and Use of Laboratory animals of the National Institutes of Health. The protocols were
 137 approved by the Animal Care and Use Committee (ACUC) of [Author Institution].

138 To fluorescently label LC-NE neurons with tdTomato, B6.Cg-Gt(ROSA)26Sor^{tm1.1(CAG-}
 139 ^{tdTomato,-EGFP)Pjen} mice (RC::RFLTG; Jackson Laboratory stock no. 026930) (Plummer et al., 2015)
 140 were intercrossed with B6.129-En1^{tm1.1(dreo)Pjen} (En1^{Dre}; Jackson Laboratory Stock no. 033953)
 141 (Plummer et al., 2016) and B6;129-Dbh^{tm1(flpo)Pjen} mice (Dbh^{Flpo}; Jackson Laboratory Stock no.
 142 033952) (Robertson et al., 2013), generating triple heterozygotes. To subsequently label
 143 subpopulations of those LC-NE neurons with EGFP based on their axonal projection pattern,
 144 En1^{Dre}; Dbh^{Flpo}; RC::RFLTG triple heterozygotes were stereotactically injected in mPFC or M1
 145 with the CAV2-Cre canine adenoviral vector (Hnasko et al., 2006).

146

147 Surgery

148 Male and female mice were deeply anesthetized through isoflurane inhalation (4%) and
 149 placed in a stereotaxic frame. Isoflurane concentration was decreased to 2.5% after reaching a
 150 surgical plane of anesthesia. Body temperature was monitored and controlled throughout the
 151 surgical procedure. Surgery was performed in flat skull orientation such that bregma and
 152 lambda were level. The dorsoventral coordinate position of each was measured, and if they
 153 were found to be >0.1mm apart, the position of the nose cone was adjusted until they were
 154 level. Stereotaxic coordinates for viral infusions were as follows, in mm, from bregma: mPFC:

155 AP +1.95, ML +0.9, DV -2.5 @ 15° from the brain surface; M1: AP +0.26, ML +1.2, DV -0.63
156 from the brain surface. All infusions were made into the left hemisphere. After drilling a small
157 craniotomy above either region, a 31 gauge Hamilton 1µL Neuros syringe (part #7001) mounted
158 on a World Precision Instruments stereotaxic syringe pump (model UMP3) was gradually
159 lowered into the brain. 0.2 µL CAV2-CMV-Cre (5.6×10^{12} pfu/mL) was injected into either region
160 at a flow rate of 0.5µL/min using a World Precision Instruments Micro4 MicroSyringe Pump
161 Controller. The needle remained in place undisturbed for 10 minutes upon completion of the
162 injection before being gradually withdrawn. Craniotomies were then filled with sterile bone wax
163 and the incision was closed with wound clips. After surgery was complete, mice were returned
164 to their home cages.

165

166 **Tissue Collection**

167 Six weeks after viral injection, mice were anesthetized with sodium pentobarbital and
168 transcardially perfused with 4% paraformaldehyde (PFA) in 0.01 M phosphate buffered saline
169 (PBS). Dissected brains were postfixed by immersion in 4% PFA at 4 °C. Brains to be sectioned
170 were marked on the uninjected hemisphere with black TMD Tissue Marking Dye (General Data
171 Company, Cincinnati, OH), equilibrated in 30% sucrose in PBS at 4 °C, and embedded in
172 Tissue Freezing Medium (General Data Company). Free-floating 40-µm sections were collected
173 in PBS and then stored at -80 °C in 30% sucrose/30% ethylene glycol in PBS. For the passive
174 clarity technique (PACT) (Yang et al., 2014), 3-mm thick slices containing the LC were cut using
175 a stainless-steel coronal brain matrix (Zivic Instruments, Pittsburgh, PA) and the remaining
176 forebrain was embedded for sectioning as described above. PACT tissue clearing was
177 performed as previously described (Plummer et al., 2015; Plummer et al., 2017).

178

179 **Immunohistochemistry**

180 We used immunofluorescent labeling to enhance signal from fluorescent proteins in fixed
 181 tissue. For simultaneous detection of virally-transduced (EGFP-labeled) and non-transduced
 182 (tdTomato-labeled) LC-NE axons, a chicken anti-GFP antibody (1:10,000; Cat.# ab13970,
 183 Abcam) was used in conjunction with Alexa Fluor 488 goat anti-chicken secondary antibody
 184 (1:1000; Cat. # A11039, Thermo Fisher Scientific, Waltham, MA), and a rabbit anti-dsRed
 185 antibody (1:500; Cat. # 632496, Clontech Laboratories, Mountain View, CA) was used with
 186 Alexa Fluor 568 goat anti-rabbit secondary antibody (1:1000; Cat. # A11036, Thermo Fisher
 187 Scientific). Mouse monoclonal anti-NET antibody (1:1000; clone NET-05; Cat. # 1447-NET,
 188 PhosphoSolutions, Aurora, CO) (Matthies et al., 2009) was used with Alexa Fluor 633 goat anti-
 189 mouse secondary antibody (1:1000; Cat. # A21052, Thermo Fisher Scientific). Tissue was
 190 incubated with primary antibodies for 2 days at 4 °C and with secondary antibodies for 2 hours
 191 at room temperature. Following antibody incubations, sections were incubated for 1 hour in a
 192 1:50 dilution of Neurotrace 435/455 Blue Fluorescent Nissl Stain (Thermo Fisher Scientific) for
 193 detection of neuronal cell bodies.

194 For immunofluorescent labeling after PACT tissue clearing, we used chicken anti-GFP
 195 (1:1000) and rabbit anti-dsRed (1:500) primary antibodies, followed by Alexa Fluor 488 donkey
 196 anti-chicken F(ab')₂ fragments (1:500; Cat. # 703-546-155, Jackson ImmunoResearch
 197 Laboratories, West Grove, PA) and Alexa Fluor 568 donkey anti-rabbit F(ab')₂ fragments
 198 (1:500; Cat. # Ab175694, Abcam, Cambridge, MA). Incubations were performed at room
 199 temperature for six days, with antibody replaced by fresh solution after three days.

200

201 **Digital Image Collection**

202 LC-NE neurons in PACT-cleared tissue or 40-μm sections were imaged on an LSM 780
 203 or 880 inverted confocal microscope (Carl Zeiss Microscopy, Thornwood, NY), using an EC
 204 Plan-Neuofluar 10x/0.30 M27 objective. For imaging axonal fibers, z-stack images through the
 205 full thickness of each 40-μm section were collected on an LSM 880 confocal microscope using a

206 PLAN Apochromat 20x/0.8 M27 or Plan Aproxchromat 40x/1.3 Oil M27 objective. Alexa Fluor
 207 633 fluorescence was excited with a 633 nm laser (pinhole setting 1 airy unit), and fluorescent
 208 emission was collected with a 640-758 nm filter. Alexa Fluor 568 fluorescence was excited with
 209 a 561 nm laser and collected with a 571-633 nm filter. Alexa Fluor 488 was excited with a 488
 210 nm laser and collected with a 491-562 nm filter, and also with a 571-633 nm filter for an
 211 autofluorescence-only channel to permit DEFINE image processing (Powell et al., 2019). Blue
 212 Nissl fluorescence was excited with a 405 nm laser and collected with a 415-470 nm filter. For
 213 fiber quantification, each anatomical region was imaged from at least three sections. The
 214 investigator was blind to labeled fibers during selection of the regions to be imaged. Location
 215 was determined by external marking with Tissue Marking Dye (see Tissue Collection, above)
 216 and by anatomy, as revealed by labeling with Nissl stain, compared to a mouse brain atlas
 217 (Paxinos and Franklin, 2013).

218

219 **Image Processing and quantification of LC neurons and axons**

220 LC neurons were quantified from a total of four mice for each injection site (from 40- μ m
 221 sections, n=2 mPFC injections and n=1 M1 injection; and from 40- μ m “virtual” sections of
 222 PACT-cleared tissue, n=2 mPFC injections and n=3 M1 injections). For counting LC-NE
 223 neurons in 40- μ m sections, z-stack images were collected from every fourth section through the
 224 full rostrocaudal extent of the fluorescently labeled LC. Maximum-intensity projections (MIP)
 225 were imported into FIJI software (Schindelin et al., 2012) for counting. Images collected from
 226 tissue cleared by PACT were viewed with Imaris software (Bitplane, Concord, MA) for three-
 227 dimensional rendering of the entire region and collection of 40- μ m virtual sections using the
 228 Ortho Slicer function. Virtual sections spaced 160 μ m apart to match the sectioned tissue were
 229 imported into FIJI for cell counting.

230 For axon quantification, z-stack images collected with the 20x objective were first
 231 cropped to the center six z-slices to ensure that the same volume of tissue would be compared

232 in all images and to exclude autofluorescent particles such as dust or secondary antibody
233 conglomerates lying between the tissue and coverslip. 400 x 400 μm areas from larger images
234 were selected for quantification, again using Nissl stain for identification of anatomic regions.
235 This fixed size was chosen in order to maximize the volume quantified while remaining within
236 the boundaries of regions defined by the mouse brain atlas (Paxinos and Franklin, 2013). To
237 minimize the effects of possible variation in axon density within an anatomic brain region, axons
238 were quantified in three sections from each region.

239 Prior to quantification, images were processed using the DEFiNE macro for Fiji (Powell
240 et al., 2019) to remove autofluorescence and other fluorescent artifacts which would affect fiber
241 density measurements. Images used as illustrations in figures were further processed only by
242 adjusting brightness and contrast across the entire image. After conversion of the processed z-
243 stack to a MIP, the DEFiNE Quantify Fibers function (Powell et al., 2019) was used to determine
244 the relative density of GFP- and tdTomato-labeled axons. The processed images were
245 converted to binary at a threshold cutoff of 4 standard deviations above mean background pixel
246 intensity, and the quantity of labeled axonal fibers was calculated as the sum of pixels remaining
247 in the three images from each anatomical region. This calculation thus reflects both fiber density
248 and caliber. To quantify the GFP-labeled axons as a percentage of total LC inputs to a region,
249 the number of GFP pixels was divided by the sum of GFP and tdTomato pixels. Fractional
250 innervation by the retrogradely labeled subpopulations across anatomical regions was
251 calculated as the number of GFP pixels in a particular region divided by the number of GFP
252 pixels in all regions imaged (Schwarz et al., 2015). Similarly, fractional innervation by the LC as
253 a whole was calculated as the sum of GFP and tdTomato pixels in a region divided by the sum
254 of GFP and tdTomato pixels in all regions.

255

256 **Statistical analysis and graphing**

257 All data are expressed as the mean \pm standard error (SEM). Unpaired t-tests, two-way
 258 ANOVA, and graphing were performed using GraphPad Prism 7 (Graphpad Software Inc., La
 259 Jolla, CA) and Microsoft Excel (Microsoft Corporation, Redmond, WA). The number of subjects
 260 and specific statistical analyses used in each experiment are indicated in the text and figure
 261 legends.

263 RESULTS

264 Current viral genetic strategies for mapping efferent projections obtain cellular specificity
 265 via injection of two viruses—one into the target region and a second in the cell population of
 266 interest—increasing the chance of variable targeting. To remove one of these variables and
 267 allow reproducible targeting of genetically defined populations of neurons, we developed the
 268 TrAC strategy. TrAC requires three basic elements: 1) a cell-type specific recombinase driver
 269 allele, 2) a dual or triple recombinase-responsive fluorescent indicator allele capable of labeling
 270 axons upon recombinase activation, and 3) a virus for retrograde delivery of one of the
 271 recombinases (Figure 1). When combining these elements, the virally-delivered recombinase is
 272 injected into the target region of interest of a transgenic mouse expressing the cell-type specific
 273 recombinase(s) and dual or triple recombinase-responsive fluorescent indicator (Figure 1).
 274 Upon recombination of the indicator allele by the retrogradely delivered recombinase, only
 275 genetically-defined cells projecting to that target region as well as their axons and collaterals will
 276 be marked by the fluorescent reporter (Figure 1).

277 To apply TrAC to the LC-NE system, we needed a way to label LC-NE neurons in
 278 isolation from other noradrenergic neuron populations. The anatomically defined LC is located in
 279 the central gray of the pons adjacent to the lateral edge of the fourth ventricle (Grzanna and
 280 Molliver, 1980). Ventrally, the more scattered neurons of the subcoeruleus, separated into
 281 dorsal and ventral subdivisions by their position relative to the motor nucleus of the trigeminal,
 282 form a continuum between the LC and the more rostral A7 and ventral A5 noradrenergic nuclei

283 (Paxinos and Franklin, 2013; Aston-Jones, 2004). We exploited the fact that 99.6% of the
 284 anatomically defined LC, together with smaller portions of the dorsal subcoeruleus and A7
 285 immediately adjacent to and continuous with the LC, share a history of the transcription factor
 286 engrailed-1 (*En1*) and the noradrenergic marker dopamine- β -hydroxylase (*Dbh*) (Robertson et
 287 al., 2013). In contrast to viral targeting, use of this genetic classification allows restricted and
 288 reproducible targeting of a subpopulation of noradrenergic neurons that closely matches the
 289 anatomically defined LC. To label the genetically defined LC-NE neurons in mice, we crossed
 290 *En1^{Dre}* and *Dbh^{Flpo}* to a triple recombinase-responsive indicator (*RC::RFLTG*; Plummer et al.,
 291 2015). In *En1^{Dre}; Dbh^{Flpo}; RC::RFLTG* triple transgenic (TrAC-LC) mice, tdTomato expression is
 292 restricted to genetically defined LC-NE neurons, switching to EGFP only upon retrograde
 293 delivery of Cre recombinase (Figure 2A).

294 To identify the LC-NE neurons projecting to the mPFC, we injected canine adenovirus
 295 encoding Cre recombinase (CAV2-CMV-Cre) into the mPFC of TrAC-LC and Flp-negative
 296 littermate control mice and examined fluorescence (Figure 2A). We found mPFC-projecting NE
 297 neurons (EGFP+) intermingled among tdTomato+ NE neurons within the LC (Figure 2B).
 298 Ipsilateral to the injection site, we counted an average of 140 ± 16 mPFC-projecting (EGFP+) and
 299 476 ± 18 tdTomato+ NE neurons, indicating that CAV2-Cre injection in the mPFC labeled
 300 $22.54 \pm 1.9\%$ of the ipsilateral LC. Contralateral to the injection site, we observed much sparser
 301 labeling, with 20 ± 6 mPFC-projecting (EGFP+) NE neurons intermingled among 519 ± 47
 302 tdTomato+, indicating that the CAV2-Cre labeled $3.83 \pm 1.3\%$ of the contralateral LC. Thus,
 303 87.5% (140/160) of the retrogradely labeled neurons were ipsilateral to the injection site, and
 304 12.5% (20/160) were contralateral to the injection site. This distribution is similar to that reported
 305 in previously published reports of LC projections to cortical targets using conventional
 306 retrograde tracer techniques (Simpson et al., 1997; Chandler and Waterhouse, 2012; Chandler
 307 et al., 2014).

308 To investigate the distribution of EGFP+ retrogradely labeled mPFC-projecting NE
309 neurons within the LC, we quantified them as a percentage of all labeled neurons (EGFP +
310 tdTomato) in three anatomic domains: the caudal core of the anatomically defined LC, the
311 rostral extension of the anatomically defined LC (Grzanna and Molliver 1980), and the
312 subcoeruleus/A7. Ipsilateral to the injection site, EGFP+ mPFC-projecting neurons were
313 distributed throughout the rostrocaudal extent of the anatomically defined LC, but they
314 constituted a greater percentage of the rostral extension than the core ($37.13 \pm 4.67\%$ rostral
315 extension, $22.55 \pm 2.90\%$ core; $p = 0.0378^a$, unpaired t-test). In contrast, EGFP+ mPFC-projecting
316 NE neurons were generally absent from the anatomically defined subcoeruleus/A7 (two mice
317 had 1 EGFP+ neuron). Although there were far fewer EGFP+ neurons in the contralateral
318 anatomically defined LC, compared to the ipsilateral, their rostrocaudal distribution appeared to
319 be the same. As expected, no EGFP+ NE-neurons were observed in Flp-negative littermate
320 control mice.

321 Next, we analyzed the distribution of axons and collaterals from the retrogradely labeled
322 mPFC-projecting LC-NE neurons in select brain regions (Figure 3). We confirmed noradrenergic
323 identity of the fluorescently labeled axons by immunostaining with an anti-norepinephrine
324 transporter (NET) antibody (data not shown). EGFP+ collaterals were widespread in multiple
325 cortical regions, including the motor, cingulate, insular and piriform cortices. In addition, we
326 observed collaterals in multiple subcortical regions, including the BNST, hippocampus,
327 amygdala, hypothalamus, and some thalamic nuclei. Because LC-NE neurons not infected by
328 the CAV2-Cre virus express tdTomato in TrAC-LC mice, we were able to quantify axon
329 collaterals from EGFP+ mPFC-projecting LC-NE neurons as a percentage of all LC-NE inputs to
330 each target region, an analysis that was not possible in prior retrograde viral studies of LC
331 projections (Schwarz et al., 2015; Uematsu et al., 2017). The contribution from EGFP+ neurons
332 was greatest in mPFC close to the injection site ($32.7 \pm 1.8\%$). At other target sites that we
333 examined, the percent contribution from the EGP+ mPFC-projecting LC-NE neurons varied from

334 27.6±0.041% in cingulate cortex (Cg ctx) to 6.1± 0.9% in ventrolateral thalamic nucleus (VL)
 335 (Figure 3). Outside the cortex, we observed the highest percent contribution in the hippocampus
 336 (CA1; 18.6±3.8%) and paraventricular hypothalamic nucleus (PVN; 15.8±3.9%). Percent
 337 contribution in thalamic nuclei was generally low, but was consistently above the average noise
 338 in the images. (Figure 3).

339 As with the mPFC injections, CAV2-cre injection in the primary motor cortex (M1) of
 340 TrAC-LC mice labeled a greater percentage of LC-NE neurons on the ipsilateral side. We
 341 counted 108±28 M1-projecting (EGFP+) NE neurons and 571±42 tdTomato+ NE neurons
 342 ipsilateral, and 12±3 M1-projecting (EGFP+) NE neurons and 617±55 tdTomato+ NE neurons
 343 contralateral to the injection site. Thus, CAV2-Cre injection in M1 labeled 15.19±3.16% of the
 344 ipsilateral LC and 1.85±0.39% of the contralateral. Of the retrogradely labeled neurons in LC,
 345 90% (108/120) were ipsilateral to the M1 injection site and 10% (12/120) were contralateral to
 346 the injection site. Again, this distribution is similar to that reported previously for LC projections
 347 to cortical targets using conventional retrograde tracer techniques (Simpson et al., 1997;
 348 Chandler and Waterhouse, 2012; Chandler et al., 2014). As observed following injection in
 349 mPFC, the EGFP-labeled neurons were distributed throughout the rostrocaudal extent of the
 350 anatomically defined LC (Figure 4). Unlike the mPFC-projecting neurons, however, the
 351 percentage of M1-projecting (EGFP+) NE neurons was similar in the LC core and rostral
 352 extension (20.03±4.12% rostral extension, 19.49±5.82% core; $p=0.9418^b$, unpaired t-test). M1-
 353 projecting neurons, like mPFC-projecting neurons, were generally absent from subcoeruleus/A7
 354 (1 EGFP+ neuron in one mouse).

355 When we examined the distribution of axon collaterals from EGFP+ M1-projecting LC-
 356 NE neurons as a percentage of all LC inputs at target sites (Figure 5), we again observed the
 357 highest percentage of labeled axons near the injection site (M1; 33.7±3.2%). As with the mPFC
 358 injections, we observed widespread EGFP+ axon collaterals in cortical and subcortical regions,
 359 with percent contributions ranging from 27.2±1.1% in mPFC to 1.4±0.3% in anteroventral

thalamic nucleus (AV). Outside the cortex, the highest percent contribution of EGFP+ axons was observed in the bed nucleus of the stria terminalis (BNST; $10.3 \pm 0.7\%$) and lateral hypothalamus (LH; $9.4 \pm 0.4\%$). As with the mPFC-projecting subpopulation, axon collaterals from M1-projecting neurons constituted a small percentage of all LC-NE inputs to thalamic nuclei (Figure 5). Although contribution from mPFC-projecting neurons was consistently above the average noise (Figure 3), that from the M1-projecting neurons was at or below the average noise level in all thalamic nuclei that we examined (Figure 5). This very sparse innervation of the thalamus by the M1-projecting LC subpopulation is notable, given that the LC is the major source of noradrenergic inputs to many thalamic nuclei (Robertson et al., 2013), including several that we examined (e.g. AV, VL, VM). In thalamic regions that receive significant non-LC noradrenergic input (e.g. PV) (Robertson et al., 2013), collaterals from the M1-projecting LC subpopulation would represent a particularly small fraction of noradrenergic inputs.

As an alternative method for analyzing the collateral data, we calculated the fractional distribution of axon collaterals across target regions (i.e. the fraction of a population of axons that innervate each target site). This method has previously been used in retrograde viral analysis of LC projections where the uninfected LC subpopulation was not labeled (Schwarz et al., 2015; Uematsu et al., 2017). Because our analysis, similar to the prior studies, quantifies a fixed volume in brain regions that differ dramatically in size and shape, this analysis reveals relative axon densities, not total axon numbers, in the brain regions. In the present study, with the whole LC labeled, we were able to compare the fractional distribution of projections from each retrogradely labeled subpopulation with that of the LC as a whole (Figure 6A-B). Compared to the retrogradely labeled subpopulations, we observed the LC as a whole projecting more uniformly to cortical and subcortical regions, though with a notably large fraction in the anteroventral thalamic nucleus. When we directly compared the distribution of axon collaterals labeled by mPFC or M1 injection (Figure 6C), we observed the fraction of EGFP+ axons to be significantly different at the injection sites ($p=0.0217^c$ mPFC and $p<0.0001^d$ M1).

386 Following injection in M1, a surprisingly large fraction of EGFP+ axons were observed in mPFC
 387 (Figure 6C), a region which may include both collaterals of M1-projecting neurons and axons of
 388 passage projecting to more caudal cortical regions (Morrison et al., 1978; Morrison et al., 1979).
 389 A greater fraction of efferents from mPFC-projecting LC-NE neurons appear to innervate the
 390 thalamus; although the difference did not reach statistical significance in individual regions that
 391 were imaged, the sum of fractional innervation of the five thalamic subregions was significantly
 392 greater for the mPFC-projecting neurons (0.1534 ± 0.0211 mPFC, 0.0773 ± 0.0119 M1;
 393 $p=0.0367^e$, unpaired t-test). Taken together, these results suggest that not only are different
 394 brain regions (e.g. M1 and mPFC) innervated by different subpopulations of LC-NE neurons, but
 395 those subpopulations differ from each other and the larger LC-NE system in their pattern of
 396 axon collateralization.

397

398 **Table 1: Statistical Table**

	Data Structure	Type of test	95% Confidence interval of difference
a	Normal	unpaired t-test	1.144 to 28.02
b	Normal	unpaired t-test	-16.90 to 17.99
c	Normal	2-way repeated measures ANOVA (Bonferroni post hoc test)	0.004639 to 0.1114
d	Normal	2-way repeated measures ANOVA (Bonferroni post hoc test)	0.08626 to 0.1930
e	Normal	unpaired t-test	0.006947 to 0.1453
See also Figure 6 legend.			

399

400 DISCUSSION

401 The noradrenergic locus coeruleus represents an extreme example of the ability of
402 projection neurons to form collateral branches. From a small population of neurons—
403 approximately ~2300 in the bilateral mouse LC (Berger et al., 1979; Touret et al., 1982;
404 Plummer et al., 2017)—a dense network of axonal fibers extends throughout the brain and
405 spinal cord. While it is clear that individual LC-NE neurons send collaterals to multiple terminal
406 fields, conventional tracing methods are not capable of identifying the degree or pattern of
407 collateralization in great detail. For example, injecting multiple retrograde tracers into discrete
408 terminal fields to identify all structures co-innervated by specific subsets of LC cells is
409 impractical since tracer uptake can be unpredictable, as well as too labor intensive for large
410 scale analyses. Recently, two newer strategies have been applied to the LC-NE system. The
411 first, MAPSeq, is a high-throughput sequencing-based approach that provides information about
412 axonal collateralization at single cell resolution, but lacks any information on the spatial
413 organization of LC neurons projecting to a given target or their axonal architecture (Kebschull et
414 al., 2016). The second strategy retains spatial information by employing a dual viral approach to
415 fluorescently label LC neurons projecting to a target brain region. This approach requires
416 retrograde delivery of a recombinase from the target structure and a recombinase-dependent
417 reporter delivered to the LC (Schwarz et al., 2015; Uematsu et al., 2017). The addition of a
418 second viral injection increases the chance of variable targeting, particularly when there is no
419 foolproof method to confirm that the virally delivered reporter is expressed in all LC-NE neurons.
420 While this method can be used successfully to target compact, anatomically discrete structures
421 like the LC, it is of limited value for the study of dispersed cell populations.

422 TrAC, on the other hand, defines the cell population of interest genetically (without
423 virus), and is not restricted by the distribution of the retrogradely labeled population, making it
424 amenable to the study of dispersed populations. Moreover, the cell population of interest is not
425 limited to cells that are defined by adult gene expression, as is the case with viral labeling.
426 Instead, the population of interest can be defined using transient developmental genetic

information. As shown in this manuscript, if the fluorescent indicator allele used in TrAC is capable of simultaneously labeling Cre⁺ and Cre-negative populations, the retrogradely labeled neurons can be directly observed in the context of the genetically defined population. In the case of complex, heterogeneous neuronal populations such as the central noradrenergic system, use of the triple recombinase responsive allele *RC::RFLTG* (Plummer et al., 2015) allows analysis to be restricted to a subset of a broader neuronal population. Thus, TrAC allowed us to observe LC axons in isolation at brain targets (e.g. BNST, PVN) that also receive significant inputs from other noradrenergic nuclei. Importantly, this method has allowed us to reliably recapitulate anatomical features that have been previously demonstrated using conventional tracers (e.g., a primarily ipsilateral projection from LC to cortex (Foote et al., 1980; Loughlin et al., 1986; Simpson et al., 1997; Chandler et al., 2014) (Figures 2 and 5), while simultaneously revealing previously inaccessible features of axonal collateralization that could not be revealed by tracer molecules.

The data presented in the current study argue for neither restricted and discrete efferent connectivity between LC neurons and their terminal fields (Chandler et al., 2013; Chandler et al., 2014), nor for a global broadcast model in which all LC neurons innervate most or all terminal fields (Aston-Jones et al., 1986; Schwarz et al., 2015). Instead, they are broadly consistent with previous analyses (Kebschull et al., 2016; Uematsu et al., 2017) indicating that axons of LC projection neurons tend to have a major terminal field destination which they densely innervate, and widespread minor terminal field targets which contain sparser axonal collaterals than the primary preferred region. Consistent with this model, we found that LC neurons projecting to mPFC have a moderate to sparse network of collaterals to other parts of the cortex and various sub-cortical locations. While the same generally holds true for cells that project to M1 cortex, one apparent deviation from this trend comes from the observation that an injection of CAV2-CMV-Cre into M1 resulted in a significantly greater fraction of EGFP⁺ axons in mPFC than an injection of the virus into mPFC (Figure 6B). While this result seems

453 paradoxical, multiple explanations are possible. One possibility is that the labeled axons
 454 observed in mPFC after injection in M1 include fibers of passage enroute to M1. Another
 455 potential explanation, which does not preclude the first, is that LC neurons innervating M1
 456 collateralize to fewer brain regions than do those innervating mPFC, resulting in a larger fraction
 457 of the total collaterals from M1-projecting neurons localized in a few target regions, with smaller
 458 fractions elsewhere. This possibility is supported by the observation that injections into M1
 459 resulted in a smaller fraction of EGFP+ axons in the thalamus as a whole, relative to injection in
 460 mPFC.

461 A question which arises from this analysis is whether or not the sparser axons that occur
 462 outside of the “primary” target do so in some organized fashion with a functional consequence;
 463 i.e., could the coordinated release of NE in mPFC and other brain regions by way of axonal
 464 collateralization have some operational role in brain function and behavior? It has been
 465 previously reported that individual LC neurons collateralize to innervate multiple structures along
 466 an ascending sensory pathway (Simpson et al., 1997), possibly as a means of simultaneously
 467 promoting NE release throughout a functional network to facilitate sensory encoding. TrAC
 468 therefore represents a viable method of identifying networks amongst which release of NE or
 469 other LC co-transmitters might occur simultaneously to facilitate a specific neurophysiological or
 470 behavioral functional role. The functional organization of LC-NE axon collaterals to cognitive,
 471 sensory and motor terminal fields can now be probed using this approach.

472 The difference in the rostrocaudal distribution of mPFC-projecting and M1-projecting
 473 neurons suggests that they constitute distinct, though overlapping, subpopulations of LC-NE
 474 neurons. However, our current inability to simultaneously label neurons projecting to two
 475 different injection sites precludes determination of the precise degree of overlap between the
 476 two subpopulations. Such analysis may become possible with a new generation of tools,
 477 including CAV2 vectors expressing recombinases other than Cre and indicator alleles like
 478 *RC::RFLTG* that express different fluorescent proteins in response to combinatorial

479 recombinase expression. Nevertheless, the current TrAC strategy, by simultaneously labeling a
 480 genetically defined neuronal population and a projection-based subpopulation, permits analyses
 481 of axon collateralization that have not previously been practicable in complex genetically and
 482 neurochemically defined neuronal subtypes.

483

484 REFERENCES

- 485 Aston-Jones G (2004) Locus coeruleus, A5 and A7 noradrenergic cell groups. In: The Rat
 486 Nervous System (Paxinos G, ed), pp253-294. San Diego, CA: Academic Press.
- 487
- 488 Aston-Jones G, Ennis M, Pieribone VA, Nickell WT, Shipley MT (1986) The brain nucleus locus
 489 coeruleus: restricted afferent control of a broad efferent network. *Science* (New York,
 490 NY) 234:734-737.
- 491 Bellesi M, Tononi G, Cirelli C, Serra PA (2016) Region-Specific Dissociation between Cortical
 492 Noradrenaline Levels and the Sleep/Wake Cycle. *Sleep* 39:143-154.
- 493 Berger B, Herve D, Dolphin A, Barthelemy C, Gay M, Tassin JP (1979) Genetically determined
 494 differences in noradrenergic input to the brain cortex: a histochemical and biochemical
 495 study in two inbred strains of mice. *Neuroscience* 4:877-888.
- 496 Bloom FE, Hoffer BJ, Siggins GR (1971) Studies on norepinephrine-containing afferents to
 497 Purkinje cells of rat cerebellum. I. Localization of the fibers and their synapses. *Brain*
 498 research 25:501-521.
- 499 Chandler D, Waterhouse BD (2012) Evidence for broad versus segregated projections from
 500 cholinergic and noradrenergic nuclei to functionally and anatomically discrete subregions
 501 of prefrontal cortex. *Front Behav Neurosci* 6:20.
- 502 Chandler DJ, Lamperski CS, Waterhouse BD (2013) Identification and distribution of projections
 503 from monoaminergic and cholinergic nuclei to functionally differentiated subregions of
 504 prefrontal cortex. *Brain research* 1522:38-58.

- 505 Chandler DJ, Gao WJ, Waterhouse BD (2014) Heterogeneous organization of the locus
 506 coeruleus projections to prefrontal and motor cortices. *Proceedings of the National*
 507 *Academy of Sciences of the United States of America* 111:6816-6821.
- 508 Chandler DJ, Jensen P, McCall JG, Pickering AE, Schwarz LA, Totah NK (2019) Redefining
 509 Noradrenergic Neuromodulation of Behavior: Impacts of a Modular Locus Coeruleus
 510 Architecture. *The Journal of neuroscience : the official journal of the Society for*
 511 *Neuroscience* 39:8239-8249.
- 512 Foote SL, Bloom FE, Aston-Jones G (1983) Nucleus locus ceruleus: new evidence of
 513 anatomical and physiological specificity. *Physiological reviews* 63:844-914.
- 514 Foote SL, Loughlin SE, Cohen PS, Bloom FE, Livingston RB (1980) Accurate three-dimensional
 515 reconstruction of neuronal distributions in brain: reconstruction of the rat nucleus locus
 516 coeruleus. *Journal of neuroscience methods* 3:159-173.
- 517 Grzanna R, Molliver ME (1980) The locus coeruleus in the rat: an immunohistochemical
 518 delineation. *Neuroscience* 5:21-40.
- 519 Hirschberg S, Li Y, Randall A, Kremer EJ, Pickering AE (2017) Functional dichotomy in spinal-
 520 vs prefrontal-projecting locus coeruleus modules splits descending noradrenergic
 521 analgesia from ascending aversion and anxiety in rats. *eLife* 6.
- 522 Hnasko TS, Perez FA, Scouras AD, Stoll EA, Gale SD, Luquet S, Phillips PE, Kremer EJ,
 523 Palmiter RD (2006) Cre recombinase-mediated restoration of nigrostriatal dopamine in
 524 dopamine-deficient mice reverses hypophagia and bradykinesia. *Proceedings of the*
 525 *National Academy of Sciences of the United States of America* 103:8858-8863.
- 526 Howorth PW, Teschemacher AG, Pickering AE (2009) Retrograde adenoviral vector targeting of
 527 nociresponsive pontospinal noradrenergic neurons in the rat in vivo. *The Journal of*
 528 *comparative neurology* 512:141-157.

529 Kebschull JM, Garcia da Silva P, Reid AP, Peikon ID, Albeanu DF, Zador AM (2016) High-
530 Throughput Mapping of Single-Neuron Projections by Sequencing of Barcoded RNA.
531 Neuron 91:975-987.

532 Li Y, Hickey L, Perrins R, Werlen E, Patel AA, Hirschberg S, Jones MW, Salinas S, Kremer EJ,
533 Pickering AE (2016) Retrograde optogenetic characterization of the pontospinal module
534 of the locus coeruleus with a canine adenoviral vector. Brain research 1641:274-290.

535 Loughlin SE, Foote SL, Bloom FE (1986) Efferent projections of nucleus locus coeruleus:
536 topographic organization of cells of origin demonstrated by three-dimensional
537 reconstruction. Neuroscience 18:291-306.

538 Matthies HJ, Han Q, Shields A, Wright J, Moore JL, Winder DG, Galli A, Blakely RD (2009)
539 Subcellular localization of the antidepressant-sensitive norepinephrine transporter. BMC
540 Neurosci 10:65.

541 McCall JG, Siuda ER, Bhatti DL, Lawson LA, McElligott ZA, Stuber GD, Bruchas MR (2017)
542 Locus coeruleus to basolateral amygdala noradrenergic projections promote anxiety-like
543 behavior. eLife 6.

544 Morrison JH, Molliver ME, Grzanna R (1979) Noradrenergic innervation of cerebral cortex:
545 widespread effects of local cortical lesions. Science (New York, NY) 205:313-316.

546 Morrison JH, Grzanna R, Molliver ME, Coyle JT (1978) The distribution and orientation of
547 noradrenergic fibers in neocortex of the rat: an immunofluorescence study. The Journal
548 of comparative neurology 181:17-39.

549 Paxinos G, Franklin KBJ (2013) The Mouse Brain in Stereotaxic Coordinates. San Diego, CA:
550 Academic Press.

551 Plummer NW, de Marchena J, Jensen P (2016) A knock-in allele of En1 expressing dre
552 recombinase. Genesis 54:447-454.

- 553 Plummer NW, Scappini EL, Smith KG, Tucker CJ, Jensen P (2017) Two Subpopulations of
 554 Noradrenergic Neurons in the Locus Coeruleus Complex Distinguished by Expression of
 555 the Dorsal Neural Tube Marker Pax7. *Front Neuroanat* 11:60.
- 556 Plummer NW, Evsyukova IY, Robertson SD, de Marchena J, Tucker CJ, Jensen P (2015)
 557 Expanding the power of recombinase-based labeling to uncover cellular diversity.
 558 *Development (Cambridge, England)* 142:4385-4393.
- 559 Powell JM, Plummer NW, Scappini EL, Tucker CJ, Jensen P (2019) DEFiNE: A Method for
 560 Enhancement and Quantification of Fluorescently Labeled Axons. *Front Neuroanat*
 561 12:117.
- 562 Robertson SD, Plummer NW, de Marchena J, Jensen P (2013) Developmental origins of central
 563 norepinephrine neuron diversity. *Nature neuroscience* 16:1016-1023.
- 564 Schindelin J, Arganda-Carreras I, Frise E, Kaynig V, Longair M, Pietzsch T, Preibisch S,
 565 Rueden C, Saalfeld S, Schmid B, Tinevez JY, White DJ, Hartenstein V, Eliceiri K,
 566 Tomancak P, Cardona A (2012) Fiji: an open-source platform for biological-image
 567 analysis. *Nat Methods* 9:676-682.
- 568 Schwarz LA, Miyamichi K, Gao XJ, Beier KT, Weissbourd B, DeLoach KE, Ren J, Ibanes S,
 569 Malenka RC, Kremer EJ, Luo L (2015) Viral-genetic tracing of the input-output
 570 organization of a central noradrenaline circuit. *Nature* 524:88-92.
- 571 Simpson KL, Altman DW, Wang L, Kirifides ML, Lin RC, Waterhouse BD (1997) Lateralization
 572 and functional organization of the locus coeruleus projection to the trigeminal
 573 somatosensory pathway in rat. *The Journal of comparative neurology* 385:135-147.
- 574 Touret M, Valatx JL, Jouvet M (1982) The locus coeruleus: a quantitative and genetic study in
 575 mice. *Brain research* 250:353-357.
- 576 Uematsu A, Tan BZ, Johansen JP (2015) Projection specificity in heterogeneous locus
 577 coeruleus cell populations: implications for learning and memory. *Learning & memory*
 578 (Cold Spring Harbor, NY) 22:444-451.

579 Uematsu A, Tan BZ, Ycu EA, Cuevas JS, Koivumaa J, Junyent F, Kremer EJ, Witten IB,
580 Deisseroth K, Johansen JP (2017) Modular organization of the brainstem noradrenaline
581 system coordinates opposing learning states. *Nature neuroscience* 20:1602-1611.
582 Yang B, Treweek JB, Kulkarni RP, Deverman BE, Chen CK, Lubeck E, Shah S, Cai L,
583 Gradinaru V (2014) Single-cell phenotyping within transparent intact tissue through
584 whole-body clearing. *Cell* 158:945-958.

585

586 FIGURE LEGENDS

587 **Figure 1: TrAC (Tracing Axon Collaterals) permits fluorescent labeling of genetically**
588 **defined neuron populations based on axonal projections.** Schematic diagrams show a
589 simple version of TrAC using two recombinases and a dual-recombinase-responsive fluorescent
590 indicator allele. Fluorescent labeling is restricted to neurons expressing recombinase A which
591 project to the brain region injected with the retrograde-transported virus encoding recombinase
592 B.

593

594 **Figure 2: Location of mPFC-protecting noradrenergic neurons within the locus**
595 **coeruleus. (A)** Schematic diagram of the *RC::RFLTG* indicator allele and coronal schematic of
596 mouse forebrain section showing position of CAV2-Cre injection. **(B)** Representative coronal
597 sections through the rostrocaudal extent of the ipsilateral LC from a TrAC-LC mouse (40- μ m
598 free-floating sections) showing distribution of EGFP-labeled (green) and tdTomato-labeled
599 (magenta) neurons. Scale bar, 200 μ m.

600

601 **Figure 3: Distribution of axon collaterals from LC neurons projecting to mPFC.**
602 Representative fluorescent images show Cre⁺ (EGFP-labeled, green) and Cre-negative
603 (tdTomato-labeled, magenta) axons in select forebrain and midbrain regions of a TrAC-LC
604 mouse injected with CAV2-Cre in medial prefrontal cortex. Numbers in the upper right corner of

each image indicate the percent of LC-NE axons in the image that are EGFP+. The bar graph (n=4 mice) indicates percentage of LC-NE axons at each brain region that originate from EGFP+ mPFC-projecting LC-NE neurons (mean \pm SEM). The dotted line represents the noise in the green channel (average green pixel count in areas qualitatively lacking EGFP-labeled axons divided by average total pixel count). Percentages below the dotted line are indistinguishable from noise. The scale bar for fluorescent images indicates 100 μ m, and each image represents 13% of the volume quantified in the bar graph. Abbreviations: mPFC, medial prefrontal cortex; Cg Ctx, cingulate cortex; M1, primary motor cortex; BNST, bed nucleus of the stria terminalis; CA1, area CA1 of the hippocampus; BLA, basolateral amygdala; BMA, basomedial amygdala; LH, lateral hypothalamus; PVN, paraventricular hypothalamic nucleus; AV, anteroventral thalamic nucleus; PV, paraventricular thalamic nucleus; VL, ventrolateral thalamic nucleus; VM, ventromedial thalamic nucleus; MG, medial geniculate nucleus; Sup. coll., superior colliculus; SNr, substantia nigra.

Figure 4: Location of motor cortex-projecting noradrenergic neurons within the locus coeruleus. (A) Coronal schematic of mouse forebrain section showing position of CAV2-Cre injection. **(B)** Representative coronal sections through the rostrocaudal extent of the ipsilateral LC from a TrAC-LC mouse (40- μ m virtual sections from PACT-cleared tissue) showing distribution of EGFP-labeled (green) and tdTomato-labeled (magenta) neurons. Scale bar, 200 μ m.

Figure 5: Distribution of axon collaterals from LC neurons projecting to motor cortex. Representative fluorescent images show Cre+ (EGFP-labeled, green) and Cre-negative (tdTomato-labeled, magenta) axons in select forebrain and midbrain regions of a TrAC-LC mouse injected with CAV2-Cre in primary motor cortex (M1). Numbers in the upper right corner of each image indicate the percent of LC-NE axons in the image that are EGFP+. The bar graph

(n=3 mice) indicates the percentage of LC-NE axons at each target region that originate from EGFP+ M1-projecting LC-NE neurons (are mean \pm SEM). The dotted line represents the noise in the green channel (average green pixel count in areas qualitatively lacking EGFP-labeled axons, divided by average total pixel count). Percentages below the dotted line are indistinguishable from noise. The scale bar for fluorescent images indicates 100 μ m, and each image represents 13% of the volume quantified in the bar graph.

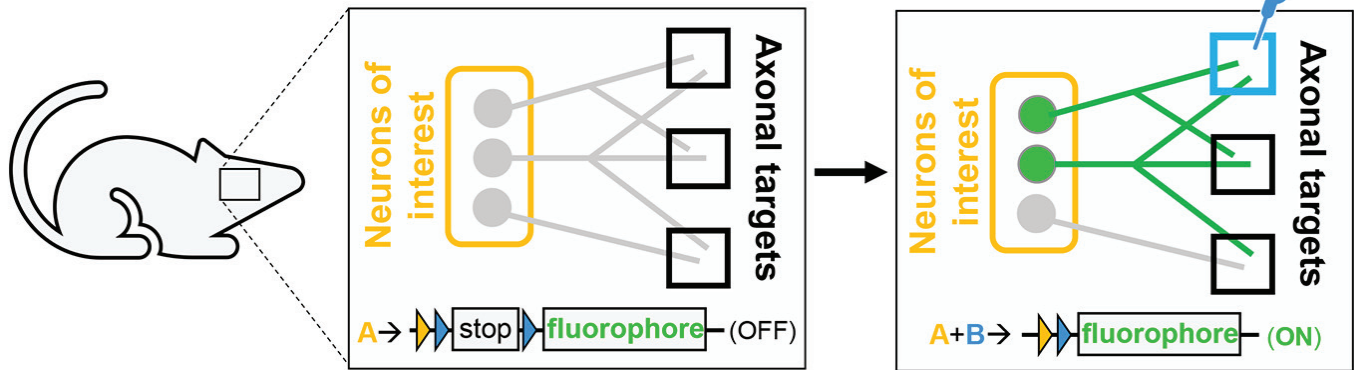
637

Figure 6: Distribution of axon collaterals from mPFC- and M1-projecting LC-NE neurons

differs from that of the LC as a whole and from each other. Bar graphs show fractional distribution of labeled mPFC-projecting, M1-projecting, or all LC-NE neurons at select target regions. Axon density at each region is represented as a fraction of labeled axons in all imaged regions. Bar graph data are mean \pm SEM and were analyzed by 2-way repeated measures ANOVA. **(A)** Comparison of mPFC-projecting (n=4 mice, EGFP+) and all LC-NE neurons (n=7 mice, sum of EGFP+ and tdTomato+ axons). LC subpopulation by target region interaction: $F_{17, 153} = 8.072$, $p < 0.0001$. Bonferroni post hoc test, **** $p < 0.0001$ (95% confidence interval of difference: mPFC -0.1441 to -0.06482, Cg Ctx -0.1059 to -0.02655, AV 0.03218 to 0.1115). **(B)** Comparison of M1-projecting (n=3 mice, EGFP+) and all LC-NE neurons (as above). LC subpopulation by target region interaction: $F_{17, 136} = 21.87$, $p < 0.0001$. Bonferroni post hoc test, * $p = 0.0176$ Cg Ctx (95% CI of diff. -0.08684 to -0.004373), * $p = 0.0117$ PV (95% CI of diff. 0.005982 to 0.08845), **** $p < 0.0001$ (95% CI of diff: mPFC -0.2037 to -0.1213, M1 -0.2007 to -0.1182, AV 0.06125 to 0.1437). **(C)** Comparison of mPFC-projecting and M1-projecting LC-NE neurons. Injection site by target region interaction: $F_{17, 85} = 5.152$, $p < 0.0001$. Bonferroni post hoc test, * $p < 0.0217$ (95% CI of diff: 0.004639 to 0.1114), **** $p < 0.0001$ (95% CI of diff: 0.08626 to 0.1930).

655

1. Cell type-specific **recombinase A** driver
2. Dual recombinase-responsive fluorescent indicator



3. Retrograde virus (**recombinase B**)



